PHYSICAL REVIEW A **79**, 031401(R) (2009)

Continuum phase shifts and partial cross sections for photoionization from excited states of atomic helium measured by high-order harmonic optical pump-probe velocity map imaging

Louis H. Haber, Benjamin Doughty, and Stephen R. Leone
Departments of Chemistry and Physics, and Lawrence Berkeley National Laboratory, University of California, Berkeley, California 94720, USA
(Received 29 September 2008; published 10 March 2009)

Phase shift differences and ratios of radial dipole matrix elements of the outgoing S and D continuum waves from state-selected helium atoms are directly measured from the photoelectron angular distributions using pump-probe velocity map imaging. Aligned $1s3p\ ^1P_1$ and $1s4p\ ^1P_1$ states in helium are prepared by high-order harmonics and ionized with either 800, 400, or 267 nm light. The results allow for the determination of energy-dependent quantum defect differences and ratios of partial cross sections and agree favorably with theoretical calculations on electron scattering and photoionization.

DOI: 10.1103/PhysRevA.79.031401 PACS number(s): 42.65.Ky, 32.10.−f, 32.80.Rm, 32.70.Fw

Measurements of the phase shifts and radial dipole matrix elements of continuum waves are necessary for complete information of a photoionization event [1,2]. The continuum wave function is the summation of individual partial waves, each with different orbital angular momenta, intensities, and phase shifts. The interference pattern of continuum partial waves produces the photoelectron angular distribution (PAD), which contains detailed information unavailable from cross section measurements alone [3]. Quantum defects [4] and partial cross sections can be determined once the phase shifts and radial dipole matrix elements are measured.

The electronically excited helium atom is an important case for investigating such complete photoionization information because its simple electronic structure allows for a detailed analysis of the partial waves from the photoelectron angular distributions. Resonant $(1+1')$ two-photon ionization from the atomic ground $^1S_0$ state in helium using collinearly polarized light creates alignment in an excited $^1P_1$ state, enabling the phase shift differences and ratios of radial dipole matrix elements to be extracted directly from the PADs of the outgoing S and D continuum waves. This situation contrasts with previous complete photoionization measurements in other atoms (e.g., alkali metals) where spin-orbit splitting causes a combination of multiple excited states, making the determination of the partial wave properties more difficult [5–9]. In addition, effects from multiple electron-electron correlations cause deviations from theoretical predictions in these larger atoms [10]. The excited helium atom has minimal electron-electron correlations, making comparisons with theoretical calculations more reliable.

The photoionization of excited states of helium is already extensively analyzed both experimentally and theoretically. Pump-probe experiments using high-order harmonics (HH) to excite helium and an optical pulse for ionization provide the total cross sections [11] and lifetimes [12] of the $1s2p\ ^1P$ and $1s3p\ ^1P$ states. Additional studies investigate the effects of spectral pulse shaping of the high-order harmonic pulse due to dispersion by the He $1s3p$ state [13]. Recent theoretical works calculate the partial cross sections from He $1s2p\ ^1P$ and $1s3p\ ^1P$ excited states [14] and the electron scattering phase shifts [14–16] for different partial waves; however, no previous experimental results verify these calculations. High-order harmonics are crucial for helium pump-probe experiments because they provide the intense pulses of extreme ultraviolet (EUV) light needed for state-selected electronic excitation with ultrafast temporal resolution and a natural synchronization with the original fundamental optical pulse.

In this paper, we use pump-probe velocity map imaging with a high-order harmonic pump pulse to excite and align helium atoms in either the $1s3p\ ^1P_1$ or $1s4p\ ^1P_1$ state and either 800, 400, or 267 nm as a probe ionization pulse. The anisotropy parameters from the photoelectron angular distributions are obtained to determine phase shift differences and ratios of the radial dipole matrix elements of the S and D partial waves as a function of photoelectron energy. The experimental results provide a fundamental test of previous theoretical predictions [14–16] and indicate excellent agreement. With available total cross section measurements, complete information is obtained on the photoionization of the $1s3p\ ^1P$ state of helium.

The experimental setup is related to those described in recent photoelectron spectroscopy studies [13,17,18]. An amplified Ti:sapphire laser system producing 2.4-mJ, 780–810 nm, 50-fs pulses at a 1-kHz repetition rate is sent to a variable beam splitter to separate pump and probe beams of controllable powers. The pump beam is focused into a pulsed Ar jet to generate high-order harmonics [16,17]. A homebuilt EUV monochromator composed of a plane grating, a plane mirror, and a toroidal mirror selects and refocuses the harmonic of interest to the interaction region. The energies of the high-order harmonics can be slightly tuned by changing the Ar gas pressure, laser intensity, and laser wavelength so that the 15th harmonic is either resonant with the He $1s^2 \rightarrow 1s3p\ ^1P_1$ transition (23.09 eV) or the $1s^2 \rightarrow 1s4p\ ^1P_1$ transition (23.74 eV). The 800-nm probe beam is sent through a retroreflector on a delay stage to control the pump-probe time delay and can also be either frequency doubled or tripled using type-1 beta barium borate (BBO) crystals. The 800, 400, or 267 nm probe pulses are focused to the interaction region to overlap with the high-order harmonic pump pulse and a skimmed atomic beam of helium. The resulting three-dimensional sphere of expanding photoelectrons is pro-

jected by an electrostatic lens to a two-dimensional position-sensitive detector in a velocity map imaging (VMI) setup [19]. Half-wave plates control the polarizations of both pump and probe pulses to be parallel to the detector face and to the direction of the atomic beam. Mu-metal surrounds the flight tube, and three orthogonal Helmholtz coils are used to eliminate magnetic fields in the interaction region. The position sensitive detector composed of two microchannel plates and a phosphor screen in front of a charge-coupled device (CCD) camera is connected to a computer to record the images.

The photoelectron images are analyzed and inverted to recover the photoelectron angular distributions. Because pump and probe photon polarizations are collinear, the photoelectron angular distributions are given by

$$I(\theta) = \frac{\sigma}{4\pi}[1 + \beta_2 P_2(\cos\theta) + \beta_4 P_4(\cos\theta)],$$

where σ is the total cross section, θ is the angle between the laser polarization and the electron velocity vector, and β_2 and β_4 are the anisotropy parameters associated with the second- and fourth-order Legendre polynomials, respectively [2]. This contrasts with single-photon ionization of randomly oriented atoms or molecules, where $\beta_4=0$ and $-1\leqslant\beta_2\leqslant 2$ [1]. The anisotropy parameters contain information on the partial wave intensities and phase shifts. Each measured photoelectron image is inverted with pBASEX software [20] using the second- and fourth-order Legendre polynomials to determine the anisotropy parameters and signal intensity at each photoelectron energy.

The inverted images from helium atoms excited to either the $1s3p\ ^1P_1$ or $1s4p\ ^1P_1$ state and ionized with either 800, 400, or 267 nm light are shown in Figs. 1(a)–1(e), with the measured anisotropy parameters listed in the caption. In addition, the inverted image from the single-photon ionization of helium with the 17th high-order harmonic is shown in Fig. 1(f), resulting in anisotropy parameters that agree with expectations for a single outgoing P wave, confirming the quantitative accuracy of the velocity map imaging setup and analysis. The laser polarization direction is vertical for each image. The radial distributions of the inverted images convert into energy spectra with the radius proportional to the photoelectron's initial speed. The energy spectra for each image are single peaks centered at 0.04, 0.70, 1.60, 2.25, 3.14, and 1.74 eV, respectively, with full width half maximum values of 0.03, 0.07, 0.22, 0.24, 0.23, and 0.21 eV, respectively. Noise in the center of each image is an artifact of the inversion. The anisotropy parameters are taken at the peak radius of each inverted image. The signal as a function of pump-probe time delay follows an error function with a rise time of approximately 100 fs due to the experiment's temporal resolution, followed by long exponential decay times of 1.7 and 3.9 ns corresponding to the lifetimes of the $1s3p$ and $1s4p$ states, respectively. To within our experimental uncertainty, there is no change in the angular distributions as a function of pump-probe time delay.

The properties of the S and D partial waves are determined from the anisotropy parameters. In the resonant two-photon photoionization of helium, the selection rules for linearly polarized photons ($\Delta L=\pm 1$, $\Delta M_L=0$) dictate the

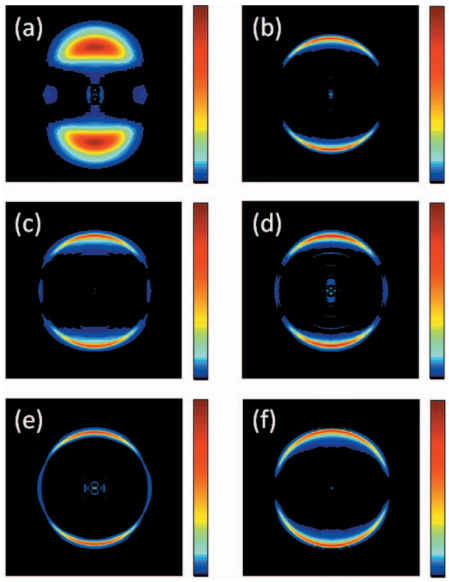

FIG. 1. (Color) Inverted photoelectron images: (a) He ($1s3p$) +800 nm, (b) He ($1s4p$)+800 nm, (c) He ($1s3p$)+400 nm, (d) He ($1s4p$)+400 nm, (e) He ($1s3p$)+267 nm, and (f) He+17th HH. The β_2 values for images (a)–(f) are 2.88 ± 0.06, 3.02 ± 0.04, 2.81 ± 0.05, 2.70 ± 0.08, 2.55 ± 0.17, and 2.03 ± 0.05, respectively. The β_4 values for images (a)–(f) are 1.93 ± 0.07, 1.64 ± 0.07, 1.88 ± 0.06, 1.72 ± 0.12, 1.78 ± 0.20, and 0.01 ± 0.02, respectively.

excited electron to be in the $m_L=0$ (P_z) orbital aligned with respect to the laser polarization. Ionization from the excited, aligned $1snp$ state by a photon with polarization collinear to the polarization of the excitation photon produces a photoelectron angular distribution proportional to $|e^{i\delta_0}D_0Y_{00} - \frac{2}{\sqrt{5}}e^{i\delta_2}D_2Y_{20}|^2$, where δ_l and D_l are the phase shift and radial dipole matrix element, respectively, of the partial wave of angular momentum l. Y_{00} and Y_{20} are spherical harmonics that depend on θ. Using the properties of spherical harmonics, the anisotropy parameters can be described by the equations

$$\beta_2 = \frac{\frac{2}{7} - X\cos\Delta}{\frac{X^2}{4} + \frac{1}{5}}, \quad \beta_4 = \frac{72}{35}\left(X^2 + \frac{4}{5}\right)^{-1},$$

where $X=D_0/D_2$ and $\Delta=\delta_0-\delta_2$.

The experimentally derived differences in phase shifts between the S and D partial waves, Δ, as a function of photoelectron energy, are shown in Fig. 2(a) and are compared to earlier theoretical work. The phase shift δ_l of each partial wave is the sum of the Coulomb phase shift and the electron scattering phase shift. The solid curve includes theoretically calculated electron scattering phase shifts from $He(1s)^+$, while the dashed curve uses a linear extrapolation of the two lowest-energy data points available from these calculations. The Coulomb phase shift can be calculated analytically and is equal to $\mathrm{Arg}[\Gamma(l+1-i\varepsilon^{-1/2})]$, where ε is the photoelectron energy in Rydbergs [1]. The Coulomb phase shift results from the hydrogenic Coulomb potential, while the electron scattering phase shift results from electron-electron interac-

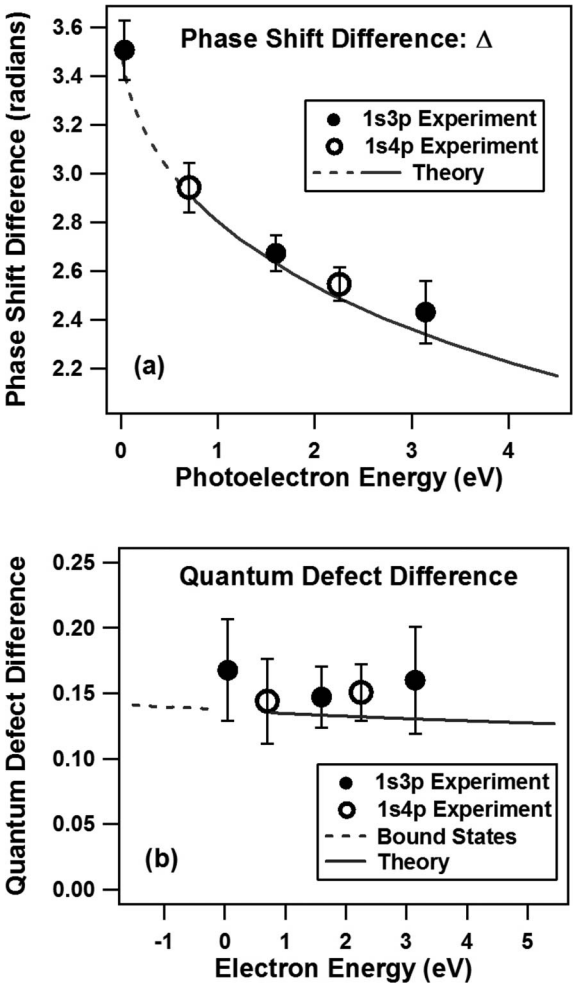

FIG. 2. The phase shift differences (a) and the quantum defect differences (b) of the S and D partial waves are extracted from the angular distributions of the inverted images. Experimental data from the He $1s3p$ and $1s4p$ states are compared to theoretically calculated values. See text for dashed and solid line descriptions in (a) and (b).

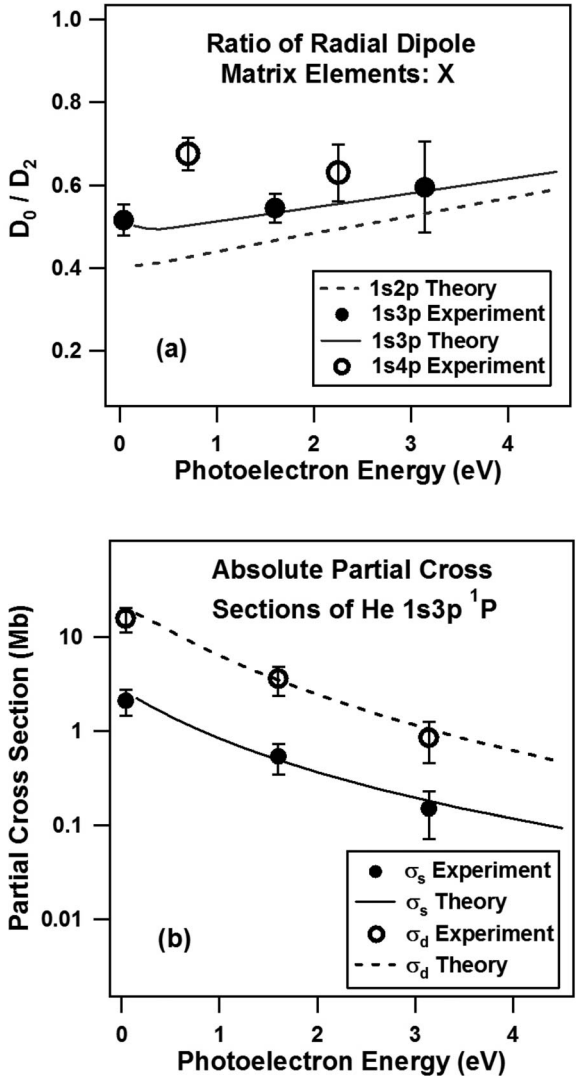

FIG. 3. (a) Ratios of radial dipole matrix elements, D_0/D_2, from S and D partial waves are extracted from the angular distributions of the inverted images. Experimental data from the He $1s3p$ and $1s4p$ states are compared to theoretically calculated values for excited He $1s2p$ and $1s3p$ states. (b) Absolute isotropic partial cross sections of the excited He $1s3p$ state to the S and D partial waves are experimentally determined and compared to theoretically calculated values.

tions. The electron scattering phase shifts calculated using the close-coupling method [15], the B-spline-based configuration-interaction method [14], and the Harris-Nesbet variational method [16] all agree well with one another for both S and D waves scattered off a $\mathrm{He}(1s)^+$ ion. All experimentally derived phase shift differences agree very well with theory, resolving ambiguities from the bivalued cosine function over the range $0-2\pi$ radians.

The quantum defect is fundamental for the description of both the bound and free atomic wave functions. The continuum-wave quantum defect differences are determined by subtracting the analytically calculated Coulomb phase shift differences from the total phase shift differences and dividing by π [4]. The experimentally derived quantum defect differences between the S and D partial waves are shown in Fig. 2(b) and are compared to results from theoretically calculated electron scattering phase shifts as well as experimentally measured and theoretically calculated bound-state quantum defects from He $1sns\ ^1S$ and $1snd\ ^1D$ Rydberg levels, for $n=3-10$ [21]. The differences of the quantum defects of the partial waves agree very well with theory and are independent of the excited state from which the continuum wave originates.

The experimentally derived ratios of the radial dipole matrix elements of the S and D partial waves, $X=D_0/D_2$, for the He $1s3p\ ^1P$ and $1s4p\ ^1P$ states are shown in Fig. 3(a) and are compared to theoretically calculated values for the He $1s2p\ ^1P$ and $1s3p\ ^1P$ states. To our knowledge, no calculations on the He $1s4p\ ^1P$ excited state radial dipole matrix elements are available. The theoretical radial dipole matrix elements are calculated using the He $1s3p\ ^1P \rightarrow {}^1S$ and $1s3p\ ^1P \rightarrow {}^1D$ nonresonant photoionization cross sections from an isotropic excited state calculated with the B-spline-based configuration interaction for photoionization wavelengths between 60 and 750 nm [14]. The total cross section from an

isotropic $1snp\ ^1P$ excited state of helium is given by $\sigma_{tot}^{iso} = \sigma_s^{iso} + \sigma_d^{iso}$, where σ_s^{iso} and σ_d^{iso} are the isotropic partial cross sections for the S and D partial waves, respectively, and $\sigma_s^{iso}/\sigma_d^{iso} = \frac{1}{2}X^2$. The total cross section for a photon of linear polarization parallel to an aligned He $1snp\ ^1P_1$ excited state is given by $\sigma_{tot}^{para} = 3\sigma_s^{iso} + \frac{6}{5}\sigma_d^{iso}$ [11]. Theoretical values of the ratios of the radial dipole matrix elements for the $1s3p\ ^1P$ state are in agreement with the experimental results. From the data obtained from the $1s4p\ ^1P$ state, the ratios of isotropic partial cross sections, $\sigma_s^{iso}/\sigma_d^{iso}$, are determined to be 0.27 ± 0.04 and 0.20 ± 0.04 for ionization with 800 and 400 nm, respectively. Including previous theoretical calculations on the partial cross sections from the $1s2p\ ^1P$ state [14], a trend of larger ratios of radial dipole matrix elements, D_0/D_2, indicating more S-wave character in the outgoing electron, is observed for higher-energy He $1snp\ ^1P$ Rydberg states.

The absolute partial cross sections can be determined using the measured ratios of the radial dipole matrix elements of the S and D continuum waves along with corresponding measurements of the absolute total photoionization cross section [11]. The total photoionization cross section of the aligned He $1s3p\ ^1P_1$ state, σ_{tot}^{para}, is measured to be 24.4 ± 6.1, 10.5 ± 2.6, and 4.2 ± 1.1 Mb at corresponding photoelectron energies of 0.15, 0.83, and 1.99 eV, respectively [11]. The cross section can be fit to the function $ln\ \sigma_{tot}^{para} = A + B\varepsilon$, where ε is the photoelectron energy in electron volts, A is 3.26 ± 0.15, and B is -0.94 ± 0.12. The extrapolated total cross section of the aligned $1s3p\ ^1P_1$ state at photoelectron energies of 0.04, 1.60, and 3.14 eV is 25.3 ± 7.3, 5.9 ± 2.0, and 1.5 ± 0.7 Mb, respectively. Using the total cross section σ_{tot}^{para} along with the measured ratios of partial cross sections, $\sigma_s^{iso}/\sigma_d^{iso}$, the absolute isotropic partial cross sections of the S and D continuum waves are determined. The results are shown in a log-linear graph in Fig. 3(b) and compare favorably to theoretically calculated values [14]. The experimentally measured partial cross sections and phase shift differences of the S and D continuum waves establish the energy-dependent complete information on the photoionization of the He $1s3p\ ^1P$ state.

The equations relating the anisotropy parameters to the partial wave properties are derived using the one-electron model [1,2], which has certain inherent deficiencies. The one-electron model describes photoionization as a one-electron process in a screened Coulomb central field, neglecting electron-electron correlations. Such a model is expected to break down near electron energy threshold or when many-electron interactions are important [10]. Large discrepancies between previous atomic complete photoionization experiments (e.g., alkali metals) and theoretical predictions are most likely due to the breakdown of the one-electron model. Helium is expected to deviate minimally from the one-electron model because electronic excitations from the ground state are highly energetic and because effects from electron-electron correlation are small. The quantitative agreement between the experimental results and previous theoretical predictions confirms the accuracy of the one-electron model of photoionization for excited helium atoms in the photoelectron energy range between 0.04 and 3.14 eV within the experimental uncertainty. Resonant $(1+1')$ two-photon ionization of an s electron from larger closed-shell atoms can also be studied using this technique, although theoretical predictions will be more difficult.

In summary, pump-probe photoelectron angular distributions from helium are measured with velocity map imaging for direct measurement of the phase shift differences and the ratios of radial dipole matrix elements of the S and D partial waves from the photoionization of $1s3p\ ^1P_1$ and $1s4p\ ^1P_1$ states. This provides a determination of the quantum defect differences and ratios of partial cross sections for photoelectron energies ranging from 0.04 to 3.14 eV. The experimental results agree with theoretically calculated values [14–16]. When incorporating these results with total cross section measurements [11], complete information on the photoionization of state-selected excited helium atoms is obtained.

The authors would like to thank Daniel Strasser, Frederick Fournier, and Oliver Gessner for their helpful discussions. The authors gratefully acknowledge financial support by the Director, Office of Science, Office of Basic Energy Sciences, Chemical Sciences, Geosciences, and Biosciences Division, U.S. Department of Energy under Contract No. DE-AC02-05CH11231.

[1] J. Cooper and R. N. Zare, Lect. Theor. Phys. **11C**, 317 (1968).
[2] S. J. Smith and G. Leuchs, Adv. At. Mol. Phys. **24**, 157 (1988).
[3] K. L. Reid, Annu. Rev. Phys. Chem. **54**, 397 (2003).
[4] M. J. Seaton, Rep. Prog. Phys. **46**, 167 (1983).
[5] H. Kaminski, J. Kessler, and K. J. Kollath, Phys. Rev. Lett. **45**, 1161 (1980).
[6] R.-L. Chien, O. C. Mullins, and R. S. Berry, Phys. Rev. A **28**, 2078 (1983).
[7] C. Kerling, N. Bowering, and U. Heinzmann, J. Phys. B **23**, L629 (1990).
[8] S. Schohl *et al.*, J. Phys. B **31**, 3363 (1998).
[9] Z.-M. Wang and D. S. Elliott, Phys. Rev. A **62**, 053404 (2000).
[10] S. T. Manson and J. W. Cooper, Phys. Rev. **165**, 126 (1968).
[11] M. Gisselbrecht *et al.*, Phys. Rev. Lett. **82**, 4607 (1999).
[12] A. Johansson *et al.*, Eur. Phys. J. D **22**, 3 (2003).
[13] D. Strasser *et al.*, Phys. Rev. A **73**, 021805(R) (2006).
[14] T. N. Chang and T. K. Fang, Phys. Rev. A **52**, 2638 (1995).
[15] D. H. Oza, Phys. Rev. A **33**, 824 (1986).
[16] T. T. Gien, J. Phys. B **35**, 4475 (2002).
[17] D. Strasser, F. Goulay, and S. R. Leone, J. Chem. Phys. **127**, 184305 (2007).
[18] S. Gilb, E. A. Torres, and S. R. Leone, J. Phys. B **39**, 4231 (2006).
[19] A. T. J. B. Eppink and D. H. Parker, Rev. Sci. Instrum. **68**, 3477 (1997).
[20] G. A. Garcia, L. Nahon, and I. Powis, Rev. Sci. Instrum. **75**, 4989 (2004).
[21] G. W. F. Drake and W. C. Martin, Can. J. Phys. **76**, 679 (1998).